Monthly Notices
of the
ROYAL ASTRONOMICAL SOCIETY

Mon. Not. R. Astron. Soc. **403,** 335–341 (2010) doi:10.1111/j.1365-2966.2009.16116.x

Relativistic Petschek reconnection with pressure anisotropy in a pair-plasma

J. M. TenBarge,⋆ R. D. Hazeltine and S. M. Mahajan

Institute for Fusion Studies, University of Texas at Austin, Austin, TX 78712, USA

Accepted 2009 November 25. Received 2009 November 24; in original form 2009 September 22

ABSTRACT

Reconnection of magnetic field lines for a wide range of parameters in the relativistic regime is considered. A newly developed covariant fluid model for magnetized plasmas, incorporating pressure anisotropy, is used to expand the study of the Petschek-type reconnection in a pair-plasma governed by slow-mode shocks. The plasma parameters are found to be strongly modified by anisotropy on both sides of the shock.

Key words: magnetic fields – MHD – shock waves.

1 INTRODUCTION

Shock-mediated reconnection is a possible source for the high-energy non-thermal emissions observed in astrophysical systems such as pulsars and magnetars (Spitovsky 2008), gamma-ray bursts (Mészáros 2006) and active galactic nuclei (Di Matteo 1998). In such strongly magnetized environments, strong gyrotropic anisotropy in the pressure is expected to occur due to synchrotron emission (Asseo & Beufils 1983) and various instabilities (Chou & Hau 2004; Daughton, Lapenta & Ricci 2004).

Petschek reconnection is a form of shock-mediated magnetic reconnection which proceeds rapidly and efficiently converts magnetic energy into thermal and bulk-flow energy (Petschek 1964). The speed of the energy conversion, inflow of the order of the Alfvén speed, is achieved by assuming the dissipation region in which the magnetic field is annihilated is small. Since the magnetic field is being annihilated, the field strength crossing from the inflow to outflow regions must drop. Further, the energy lost due to reconfiguration of the field geometry causes the temperature across the shock to rise. As such, the Petschek reconnection is governed by slow-mode shocks, which follow the above behaviour, analogous to slow-mode compressional magnetohydrodynamic (MHD) modes. We will consider a switch-off shock, a special case of a slow-mode shock in which the component of the magnetic field tangent to the shock is 'switched off' when crossing the shock.

Biskamp (1986) argues that the Petschek reconnection cannot be obtained without imposing an unphysically large (anomalous) resistivity to the diffusion region. However, slow-mode shocks have been observed in the solar corona (Shibata 1996) and via the cluster satellites in the Earth's magnetotail (Eriksson, Øieroset & Baker 2004).

Switch-off shocks in the isotropic non-relativistic limit have been explored by Biernat, Heyn & Semenov (1987). Biernat et al. (2002) extended the result to include anisotropic pressure; however, they restrict the outflowing plasma to be isotropic. Hoshino et al. (1997) perform a double adiabatic style closure to include pressure anisotropy; further, they included a phenomenological heat-flow term. They found including pressure anisotropy and heat flow allowed analytical calculations to better match data from the Earth's magnetotail taken via the GEOTAIL spacecraft.

The problem of relativistic shock-mediated magnetic reconnection was first approached by Blackman & Field (1994) and Lyutikov & Uzdensky (2003). The two approaches reached similar conclusions; however, the plasma was assumed incompressible and the full energy and momentum balance were neglected in both the cases. Tolstykh et al. (2007) extended the results of Blackman & Field (1994) and Lyutikov & Uzdensky (2003) by considering non-steady-state solutions but retained the same simplifications. Lyubarsky (2005) took a more sophisticated approach and used the relativistic generalization of the Rankine–Hugoniot shock jump relations to solve the switch-off shock Riemann problem. Double et al. (2004) studied the effect of anisotropy on relativistic shocks; however, they assume a fixed ratio of $p_\parallel/p_\perp$ to complete their closure. Recently, two groups, Swisdak, Liu & Drake (2008) and Zenitani & Hesse (2008), have begun simulating relativistic electron–positron (pair) plasma reconnection via particle-in-cell (PIC) codes, which naturally allow for pressure anisotropy. Both groups observe strong anisotropy in the outflowing plasma, giving rise to a Weibel instability that mediates the size of the diffusion region and allows fast reconnection to occur.

We present a generalization of the Petschek model to include the relativistic regime with anisotropic pressure. We employ a limit of the relativistic, magnetized fluid closure presented in TenBarge et al. (2008) to perform our analysis. It will be shown that the outflowing plasma develops a strong positive anisotropy regardless of the upstream parameters, and the compression ratio of the shock is significantly reduced in anisotropic shocks. Furthermore, the downstream plasma is found to be firehose-unstable for plasmas in which the magnetic energy is of the order the particle energy.

⋆E-mail: jason-tenbarge@uiowa.edu

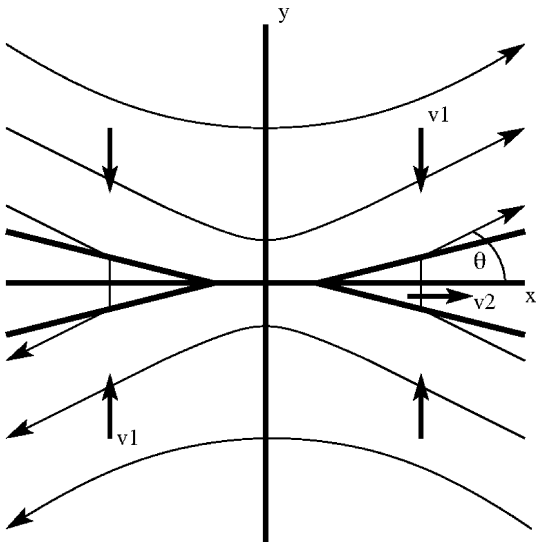

Figure 1. Shock-mediated magnetic reconnection.

We begin our analysis with a development of the conservation equations, applicable to any shock, necessary to derive the anisotropic, relativistic Rankine–Hugoniot relations for slow-mode shocks in Section 2. We briefly describe the isotropic shock limit in Section 3. In Section 4, we examine the predictions of the Rankine–Hugoniot relations analytically for the case in which the magnetic energy is much greater than the particle energy and numerically for a wide range of parameters. Our results are summarized in Section 5.

2 RELATIVISTIC SLOW-MODE SHOCKS

We begin by constructing the Rankine–Hugoniot relations for the fully relativistic pair-plasma fluid system with gyrotropic pressure anisotropy. Plasma quantities are measured in the rest frame of the plasma, and electromagnetic fields are measured in the shock frame. The Petschek-style reconnection for a slow-mode switch-off shock in the *xy*-plane is considered, as indicated in Fig. 1. Inflowing plasma is oriented normal to the shock (normal-incidence frame), and the upstream magnetic field has normal and tangential (*y* and *x*) components. The downstream plasma flow has normal and tangential components, while the downstream field will have only a normal component – a switch-off shock.

2.1 Conservation equations

The original closure presented by TenBarge et al. (2008) includes heat flow; however, we do not include heat flow in this analysis because a closure involving both heat fluxes consisting purely of conservation laws is not possible. Although the Riemann problem can be solved given a set of equations in non-conservative form, knowledge of the physics in the dissipation region is required (see e.g. LeFloch 1989). Knowledge of the dissipation region is required because the path taken by each parameter while crossing the shock cannot in general be assumed to be a straight line connecting the two sides of the shock discontinuity.

The stress-energy tensor of the plasma appearing in TenBarge et al. (2008) can be summed over species and re-expressed as

$$T_p^{\mu\nu} = \left(p - \frac{1}{3}\Delta p\right)\eta^{\mu\nu} + \left[\rho W(\zeta) - \frac{1}{3}\Delta p\right]U^\mu U^\nu + \Delta p h^\mu h^\nu/h^2, \tag{1}$$

neglecting heat flux, where $\rho W(\zeta) = mn\frac{K_3(\zeta)}{K_2(\zeta)}$ is the enthalpy density and the K_i are the MacDonald function of $\zeta = m/T = mn/p$, $p = (p_\parallel + 2\,p_\perp)/3$, $\Delta p = p_\parallel - p_\perp$, where parallel and perpendicular are with respect to the background magnetic field, $\eta^{\mu\nu}$ is the metric tensor, $U^\mu = \gamma\,(1,\,\boldsymbol{v})$ is the fluid four-velocity, $h^\mu = [\gamma\boldsymbol{B}\cdot\boldsymbol{V},\,\boldsymbol{B}/\gamma + \gamma\,(\boldsymbol{B}\cdot\boldsymbol{V})\,\boldsymbol{V}\,]$ and $h^2 = h^\mu h_\mu$. The stress-energy tensor of the electromagnetic field can be written as

$$T_{\rm EM}^{\mu\nu} = \frac{h^2}{2}\eta^{\mu\nu} + h^2U^\mu U^\nu - h^\mu h^\nu.$$

In the preceding and all following expressions, we have summed over species assuming a pair-plasma: $m_e = m_p = m/2$, $p_e = p_p = p/2$, $\Delta p_e = \Delta p_p = \Delta p/2$, $n_e = n_p = n$ and $\boldsymbol{V}_e = \boldsymbol{V}_p = \boldsymbol{V}$. We can now write the equations of particle flux

$$\partial_\mu nU^\mu = 0, \tag{2}$$

momentum

$$\partial_\mu \mathcal{T}^{\mu i} = 0 \tag{3}$$

and energy

$$\partial_\mu \mathcal{T}^{\mu 0} = 0 \tag{4}$$

in conservative form, where $\mathcal{T}^{\mu\nu} = T_p^{\mu\nu} + T_{\rm EM}^{\mu\nu}$ is the total stress tensor summed over species.

At this point, an equation for Δp is needed to close the system. To close the system, we use

$$e_{\alpha\beta}\partial_\mu M^{\mu\alpha\beta} = 0, \tag{5}$$

where $e_{\mu\nu}$ is a perpendicular projector and $M^{\alpha\beta\gamma}$ is the third-rank tensor moment, whose full expression can be found in TenBarge et al. (2008). Equation (5) can be reduced to obtain the conservation equation from Hazeltine & Mahajan (2002)

$$\partial_\mu\left(\frac{m_1U^\mu}{h}\right) = 0, \tag{6}$$

where m_1 is an auxiliary parameter found in TenBarge et al. (2008). However, we neglect terms proportional to Δp^2 appearing in m_1. These higher-order terms only need to be retained when considering heat flow, which requires fourth rank moments and implicitly includes terms second order in the anisotropy. In this reduced form,

$$m_1 = m\left(p\frac{K_3}{K_2} - \frac{1}{3}\Delta p\frac{K_4}{K_3}\right). \tag{7}$$

In three-vector form, equations (2)–(4) and (6) are

$$\partial_t(\gamma\rho) + \nabla\cdot(\gamma\rho\boldsymbol{v}) = 0 \tag{8}$$

$$\partial_t\left[\gamma^2\left(\rho W - \frac{1}{3}\Delta p\right)v^i + \Delta p k^0 k^i + (\boldsymbol{E}\times\boldsymbol{B})^i\right] + \partial_j\left[\gamma^2\left(\rho W - \frac{1}{3}\Delta p\right)v^iv^j + \left(p - \frac{1}{3}\Delta p + \frac{E^2+B^2}{2}\right)\delta^{ij} + \Delta p k^i k^j - B^iB^j - E^iE^j\right] = 0 \tag{9}$$

$$\partial_t\left[\gamma^2\left(\rho W - \frac{1}{3}\Delta p\right) - \left(p - \frac{1}{3}\Delta p\right) + \Delta p\left(k^0\right)^2 + \frac{E^2+B^2}{2}\right] + \nabla\cdot\left[\gamma^2\left(\rho W - \frac{1}{3}\Delta p\right)\boldsymbol{v} + \Delta p k^0\mathbf{k} + \boldsymbol{E}\times\boldsymbol{B}\right] = 0 \tag{10}$$

$$\partial_t\left[\frac{\gamma\,(pW + \Delta pK_4/K_3)}{h}\right] + \nabla\cdot\left[\frac{\gamma\,(pW + \Delta pK_4/K_3)\,\boldsymbol{v}}{h}\right] = 0. \tag{11}$$

Equations (8)–(11) represent a closed set of relativistic fluid conservation equations in the magnetized limit and can be straightforwardly applied to any shock type or geometry.

2.2 Rankine–Hugoniot relations

We now construct the Rankine–Hugoniot relations by considering a steady state with the geometry of a slow-mode switch-off shock and integrate equations (8)–(11) along with the relevant Maxwell equations across the shock. We find

$$[E_z] = 0, \tag{12}$$

$$[B_n] = 0, \tag{13}$$

$$[\gamma \rho v_n] = 0, \tag{14}$$

$$\left[p - \frac{1}{3}\Delta p + \gamma^2 v_n^2 \left(\rho W - \frac{1}{3}\Delta p\right) + \Delta p \frac{h_n^2}{h^2} + \frac{B_t^2 - B_n^2}{2}\right] = 0, \tag{15}$$

$$\left[\gamma^2 v_n v_t \left(\rho W - \frac{1}{3}\Delta p\right) + \Delta p \frac{h_n h_t}{h^2} - B_n B_t\right] = 0, \tag{16}$$

$$\left[\gamma^2 v_n \left(\rho W - \frac{1}{3}\Delta p\right) + \Delta p \frac{h_n h^0}{h^2} + B_t E_z\right] = 0, \tag{17}$$

$$\left[\frac{(pW + \Delta p K_4/K_3)\gamma v_n}{h}\right] = 0, \tag{18}$$

where bracketed terms are to be evaluated on each side of the shock.

The h-terms can be expressed in terms of v and B as

$$\begin{aligned}
h_{n1} &= \gamma_1 B_n \\
h_{t1} &= \frac{B_{t1}}{\gamma_1} \\
h_1^0 &= \gamma_1 v_{n1} B_n \\
h_1 &= \sqrt{B_1^2 - v_{n1}^2 B_{t1}^2} \\
h_{n2} &= \gamma_2 B_n \left(1 - v_{t2}^2\right) \\
h_{t2} &= \gamma_2 v_{2n} v_{2t} B_n \\
h_2^0 &= \gamma_2 v_{n2} B_n \\
h_2 &= B_n \sqrt{1 - v_{t2}^2},
\end{aligned} \tag{19}$$

where 1 and 2 indicate upstream and downstream of the shock, respectively, and $B_1^2 = B_n^2 + B_{t1}^2$.

We now normalize the equations and simplify to obtain our jump relations

$$B_{n1} = B_{n2} = B_n \tag{20}$$

$$v_{t2} = -v_{n1} \cot\theta \tag{21}$$

$$\frac{\rho_2}{\rho_1} = \frac{\gamma_1 v_{n1}}{\gamma_2 v_{n2}} \tag{22}$$

$$\begin{aligned}
&\frac{\gamma_1}{v_{n1}}\left[\frac{1}{\gamma_1^2}\left(\pi_1 - \frac{1}{3}\mathrm{d}\pi_1\right) + \mathrm{d}\pi_1 \frac{\sin^2\theta}{1 - v_{n1}^2\cos^2\theta}\right. \\
&\quad \left. + v_{n1}^2\left(W_1 - \frac{1}{3}\mathrm{d}\pi_1\right) + \frac{\hat{\sigma}\cos^2\theta}{2}\right] \\
&\quad = \frac{\gamma_2}{v_{n2}}\left[\frac{1}{\gamma_2^2}\left(\pi_2 + \frac{2}{3}\mathrm{d}\pi_2\right) + v_{n2}^2\left(W_2 + \frac{2}{3}\mathrm{d}\pi_2\right)\right]
\end{aligned} \tag{23}$$

$$\begin{aligned}
&\frac{\gamma_1}{v_{n1}}\left[\frac{\mathrm{d}\pi_1}{\gamma_1^2}\frac{1}{1 - v_{n1}^2\cos^2\theta} - \hat{\sigma}\right]\sin\theta\cos\theta \\
&\quad = \gamma_2 v_{t2}\left(W_2 + \frac{2}{3}\mathrm{d}\pi_2\right)
\end{aligned} \tag{24}$$

$$\begin{aligned}
&\gamma_1\left(W_1 - \frac{1}{3}\mathrm{d}\pi_1 + \mathrm{d}\pi_1\frac{\sin^2\theta}{1 - v_{n1}^2\cos^2\theta} + \hat{\sigma}\cos^2\theta\right) \\
&\quad = \gamma_2\left(W_2 + \frac{2}{3}\mathrm{d}\pi_2\right)
\end{aligned} \tag{25}$$

$$\frac{\pi_1 W_1 - \frac{1}{3}\mathrm{d}\pi_1\left(\frac{K_4}{K_3}\right)_1}{\sqrt{1 - v_{n1}^2\cos^2\theta}}\sin\theta = \frac{\pi_2 W_2 - \frac{1}{3}\mathrm{d}\pi_2\left(\frac{K_4}{K_3}\right)_2}{\sqrt{1 - v_{t2}^2}}, \tag{26}$$

where $\theta = \arctan(B_n/B_{t1})$, $\hat{\sigma} = \frac{B_1^2}{\gamma_1^2\rho_1}$, $\pi = \frac{p}{\rho} = \frac{1}{\zeta}$ and $\mathrm{d}\pi = \frac{\Delta p}{\rho}$. Note, $\hat{\sigma} = \sigma/\gamma$, where σ is parameter commonly appearing used in pulsar literature which represents the ratio of the Poynting flux to particle energy.

In the non-relativistic limit, this system reduces to the Rankine–Hugoniot relations for a double-adiabatic (Chew, Goldberger & Low 1956) plasma. As such, the system reproduces previous results in the literature (Biernat et al. 2002) when appropriate limits are taken and smoothly connects non-relativistic shock theory to a fully relativistic generalization.

3 ISOTROPIC LIMIT

In the limit with no pressure anisotropy on either side of the shock, a cold plasma upstream and a relativistically hot plasma downstream, Lyubarsky (2005) found the following inflow velocity

$$v_{n1}^2 = \frac{\hat{\sigma}\sin^2\theta}{1 + \hat{\sigma}\cos^2\theta}. \tag{27}$$

To obtain analytical results for other parameters, Lyubarsky assumes $\hat{\sigma} \gg 1$ and performs expansions to find

$$v_{n1} = \tan\theta, \tag{28}$$

$$v_{t2} = -v_{n1}\cot\theta = -\left(1 - \frac{1}{2\hat{\sigma}\cos^2\theta}\right), \tag{29}$$

$$v_{n2} = \frac{\sin\theta}{2\hat{\sigma}\cos^3\theta}, \tag{30}$$

$$\pi_2 = \frac{B_1^2\cos^2\theta}{2\rho_2} = \frac{\hat{\sigma}\gamma_1^2\cos^2\theta}{2}\frac{\rho_1}{\rho_2}, \tag{31}$$

$$\rho_2 = 2\rho_1\cos^2\theta\sqrt{\frac{\hat{\sigma}}{\cos 2\theta}}. \tag{32}$$

We reproduce these results in the limit $\Delta p_1 = \Delta p_2 = 0$ and use the results as a baseline for comparison.

4 ANISOTROPIC RESULTS

Combining equations (21), (24) and (25), we can express the inflow velocity as

$$v_{n1}^2 = \frac{\left(\hat{\sigma} - \frac{\mathrm{d}\pi_1}{\gamma_1^2}\frac{1}{1 - v_{n1}^2\cos^2\theta}\right)\sin^2\theta}{W_1 - \frac{1}{3}\mathrm{d}\pi_1 + \mathrm{d}\pi_1\frac{\sin^2\theta}{1 - v_{n1}^2\cos^2\theta} + \hat{\sigma}\cos^2\theta}. \tag{33}$$

The inflow velocity is abated when the numerator vanishes, which corresponds to the onset of the firehose instability ($B_1^2 < \Delta p_1$)

for the inflowing plasma. Note that equation (33) corresponds to the Alfvén speed in the shock frame of the plasma and has no dependence on the downstream parameters.

For the same case as considered by Lyubarsky (2005) except with the inclusion of pressure anisotropy in the downstream plasma (upstream cold and isotropic), one finds the following results:

$$\frac{\rho_2^{\Delta p}}{\rho_2} = \frac{4}{7} \qquad \frac{v_{n2}^{\Delta p}}{v_{n2}} = \frac{7}{4}$$
$$\frac{v_{n1}^{\Delta p}}{v_{n1}} = 1 \qquad \frac{\pi_2^{\Delta p}}{\pi_2} = \frac{3}{4}$$
$$\frac{v_{t2}^{\Delta p}}{v_{t2}} = 1 \qquad \frac{\mathrm{d}\pi_2^{\Delta p}}{\pi_2} = \frac{3}{2}$$
$$\frac{\mathrm{d}\pi_2^{\Delta P}}{\pi_2^{\Delta P}} = 2,$$

where $x^{\Delta p}$ represents results with downstream anisotropy. The downstream plasma is marked by the presence of a *strong pressure anisotropy which occurs regardless of the anisotropy of the upstream plasma*. Upstream pressure anisotropy plays a small role in the dynamics of the system until it is of the order of the magnetic energy, $\Delta p_1 \simeq B^2$.

4.1 Exploration of various parameter regimes

Having explored simple analytical solutions to the relativistic switch-off shock with pressure anisotropy, we now turn to examining numerical results computed via Mathematica®. We choose an intermediate shock angle of 22.5 for all of the shocks appearing in this section. All downstream parameters are plotted against the normalized upstream plasma temperature, T_1/m, so that the far left of each plot represents non-relativistic inflow temperatures.

We begin by examining three relativistic cases in which the upstream anisotropy is zero (Figs 2–4). In each log–log plot, dashed lines are results with downstream anisotropy and solid lines are fully isotropic results, while dash–dotted lines are downstream temperature anisotropy. In Fig. 2, $\hat{\sigma}$ is chosen to be an ultrarelativistic value of 100. If we define the strength of our shock by the compression ratio, ρ_2/ρ_1, we see the anisotropic shock is weaker than its isotropic counterpart. The shock is also cooler than its isotropic counterpart but features a downstream anisotropy roughly twice its temperature. The outflowing normal velocity is enhanced but remains small compared to the tangential velocity, which is unchanged in the anisotropic case since it is proportional to the inflow velocity and determined solely by upstream parameters.

Moving on to Fig. 3, for which $\hat{\sigma} = 1$, the same overall trends as the ultrarelativistic case are observed. However, the compression ratio crosses below unity for $T_1/m \gtrsim 0.45$. As in non-relativistic shocks (Zel'dovich & Raizer 2002), the second law of thermodynamics requires the compression ratio to increase across a shock due to irreversible dissipation occurring in the shock. Thus, the shock in this regime is weakened to the point of becoming continuous for temperatures above approximately 0.45 m. Further, in Fig. 4, in which the magnetic field is moderately relativistic, $\hat{\sigma} = 0.001$, the shock ceases to exist at a yet lower temperature and is significantly weaker than its isotropic counterpart.

Fig. 5 explores the effect of upstream pressure anisotropy on the switch-off shock in the relativistic regime of $\hat{\sigma} = 1$. Represented by red in this figure is the case $\Delta p_1 = p_1(p_{\parallel 1} = \frac{5}{2}p_{\perp 1})$, blue is the case $\Delta p_1 = -p_1(p_{\parallel 1} = \frac{1}{4}p_{\perp 1})$ and black has

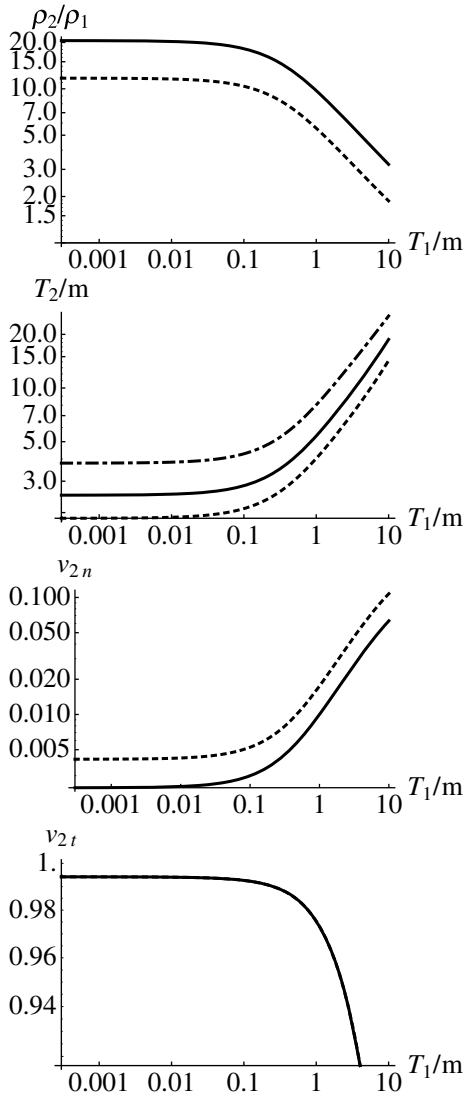

Figure 2. Log–log plot of downstream parameters of a switch-off shock with respect to upstream temperature. $\hat{\sigma} = 100, \Delta\pi_1 = 0, \theta = 22.5$. Dashed are results with downstream anisotropy and solid are fully isotropic results. Dash–dotted is downstream temperature anisotropy.

$\Delta p_1 = 0$ – all three cases permit downstream anisotropy. For non-relativistic inflow temperatures, the anisotropy of the upstream plasma plays little role in determining the downstream plasma. Also, upstream anisotropy has a negligible effect on the downstream temperature. Examining the compression ratio curves reveals positive upstream anisotropy serves to weaken the shock, while negative anisotropy strengthens and stabilizes the shock.

Fig. 6 presents the case one might expect to find in a strongly magnetized pulsar magnetosphere. Relativistically strongly magnetized plasmas will rapidly radiate away their perpendicular energy (temperature) due to synchrotron radiation (Asseo & Beufils 1983), leaving $p_{\parallel 1} \gg p_{\perp 1}$.

We take a brief aside to note the quantity $\Delta p/p$ is bounded. Explicitly,

$$\frac{\Delta p}{p} = \frac{3(p_\parallel - p_\perp)}{p_\parallel + 2p_\perp}, \tag{34}$$

which has two limits:

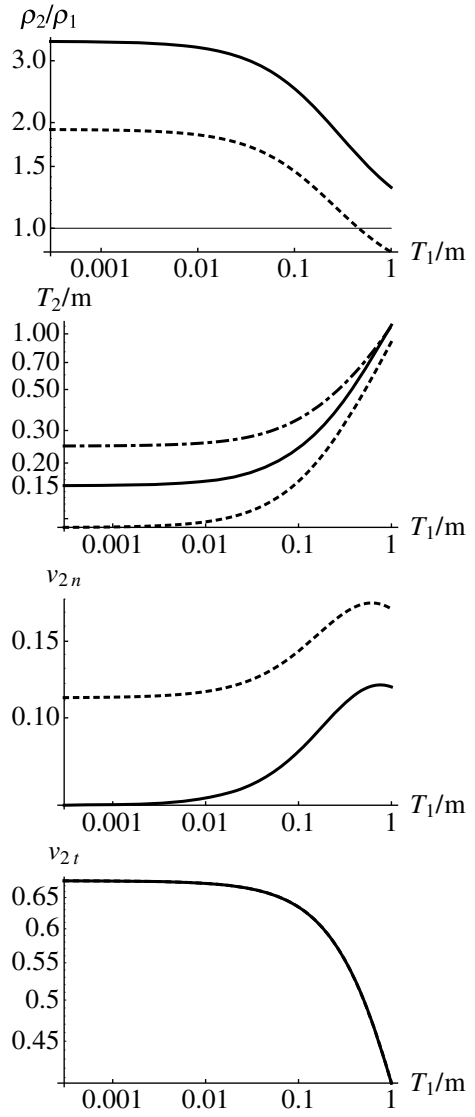

Figure 3. Log–log plot of downstream parameters of a switch-off shock with respect to upstream temperature. $\hat{\sigma} = 1, \Delta\pi_1 = 0, \theta = 22.5$. Dashed are results with downstream anisotropy and solid are fully isotropic results. Dash–dotted is downstream temperature anisotropy.

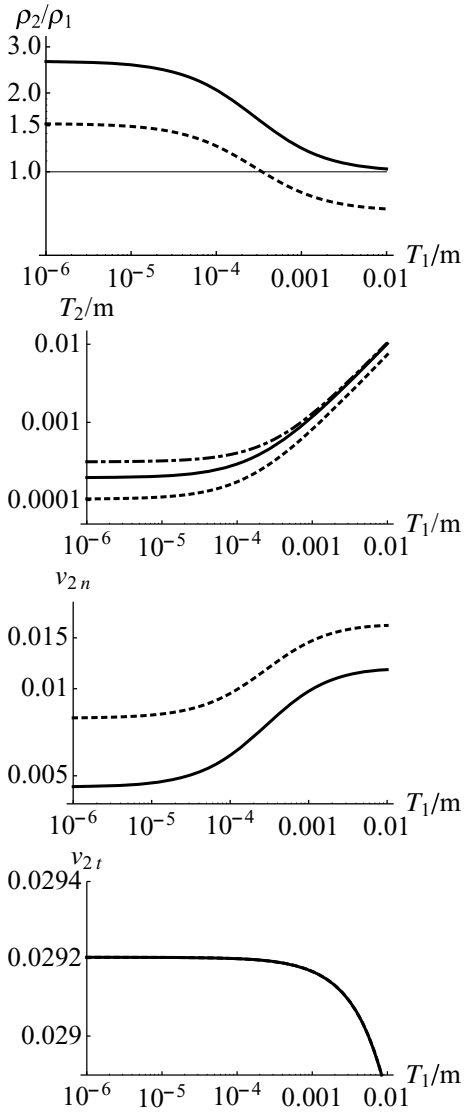

Figure 4. Log–log plot of downstream parameters of a switch-off shock with respect to upstream temperature. $\hat{\sigma} = 0.001, \Delta\pi_1 = 0, \theta = 22.5$. Dashed are results with downstream anisotropy and solid are fully isotropic results. Dash–dotted is downstream temperature anisotropy.

(i) $p_\parallel \gg p_\perp$: in which case $\Delta p/p \to 3$;
(ii) $p_\parallel \ll p_\perp$: in which case $\Delta p/p \to -3/2$.

Therefore, $\Delta p/p \in (-3/2, 3)$.

In Fig. 6, dashed lines represent the case which is likely to be seen in a pulsar magnetosphere with anisotropy up- and downstream (dash–dotted line), solid lines represent an isotropic upstream plasma with only downstream anisotropy (dotted line). As noted above but enhanced by the stronger positive anisotropy, the shock in the pulsar case is weaker than the isotropic case and shuts off above $T_1 \simeq 0.1m$ for this parameter regime. The shut off suggests this form of shock may not occur in the relativistically hot and magnetized regions of pulsar and magnetar magnetospheres.

A strong anisotropy downstream of a pair-plasma reconnection event has been observed in PIC simulations performed by Swisdak et al. (2008) and Zenitani & Hesse (2008). In their simulations, they observed a maximum downstream anisotropy of $T_{tt}/T_{nn} \simeq 4$, where T is the stress tensor of the plasma. Also observed was an enhancement of the out-of-plane magnetic field. They argue that the anisotropy drives a Weibel instability in the downstream plasma whose generated turbulence serves to limit the length of the reconnection current sheet, thereby facilitating fast reconnection. The source of the Weibel instability is the two 'streams' of plasma having different temperatures. In non-relativistic pair-plasma simulations, Daughton & Karimabadi (2007) observed the possible signature of a firehose instability in the strongly anisotropic downstream pair-plasma. The role the instability played in the reconnection dynamics was not explored. Further, evidence of firehose unstable plasma downstream of a slow-mode shock was observed in ISEE 2 data (Walthour, Sonnerup & Russell 1995).

In our case, $T_{tt}/T_{nn} \simeq 1/7 + 10\gamma_2^2 v_{t2}^2/7$ for the relativistically strongly magnetized shocks with relativistic downstream temperatures considered in our analysis. For the cases considered herein, T_{tt}/T_{nn} can be of the order of 100. An out-of-plane magnetic field was not included in our analysis; however, the Weibel instability in the form of two warm streams is a purely kinetic instability. The

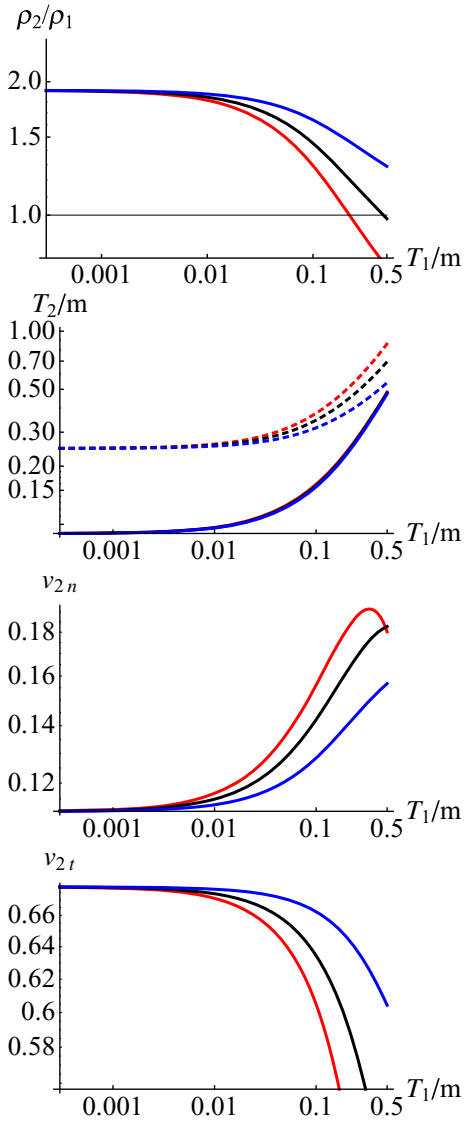

Figure 5. Effect of Upstream Anisotropy ($\hat{\sigma} = 1, \theta = 22.5$). Cases: Red = $\mathrm{d}\pi_1 = \pi_1$, Blue = $\mathrm{d}\pi_1 = -\pi_1$, = $\mathrm{d}\pi_1 = 0$. Dashed represents $\mathrm{d}\pi_2$ in all cases.

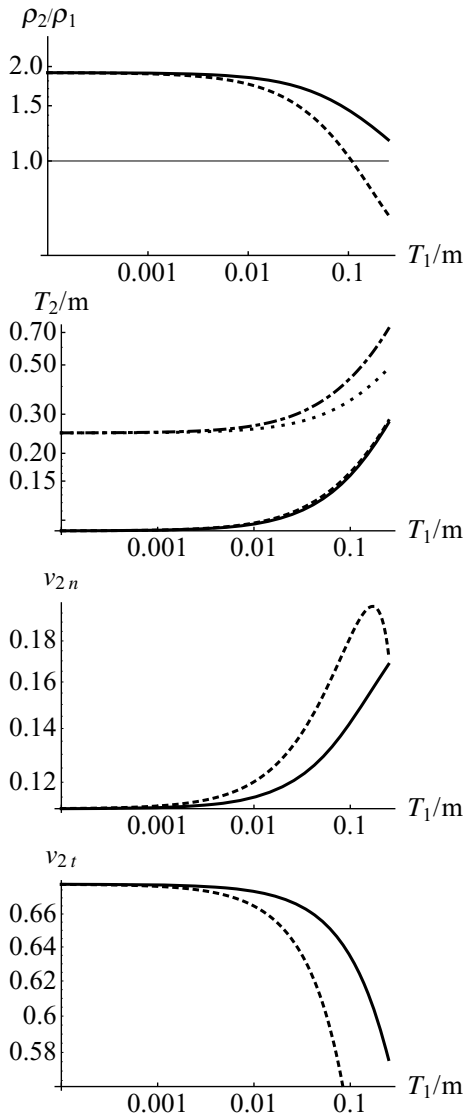

Figure 6. Pulsar/Magnetar Case ($\hat{\sigma} = 1, p_{\parallel 1} \gg p_{\perp 1}, \theta = 22.5$). All results calculated allow for downstream anisotropy. Dashed are results with upstream anisotropy, $\mathrm{d}\pi_1 = 3\pi_1$, and solid have upstream isotropy. Dash–dotted is downstream temperature anisotropy for the full anisotropy case and dotted is downstream anisotropy for the case with upstream isotropy.

only fluid analogue progenitor of a Weibel instability is to impose cold beams on the plasma.

Although we cannot observe a Weibel-like instability in our fluid approach, we can examine the firehose instability. In all parameter regimes explored, the downstream plasma exhibits a positive anisotropy on the order of the downstream temperature. Since the firehose instability threshold is unmodified for relativistic plasmas (Chou & Hau 2004), the threshold for the downstream plasma can be expressed as

$$\frac{B_2^2}{\rho_2} - \frac{\Delta p_2}{\rho_2} = \hat{\sigma} \sin^2\theta \frac{\gamma_1 \gamma_2 v_{n2}}{v_{n1}} - \mathrm{d}\pi_2 < 0, \tag{35}$$

the strong positive anisotropy produced by the shock results in a firehose unstable plasma for relativistically strongly magnetized ($\hat{\sigma} = \frac{B_1^2}{\gamma_1^2 \rho_1} \gtrsim 1$) upstream plasma. This instability likely leads to turbulence in the outflowing plasma, which may play the same role as the Weibel instability for these relativistic cases.

5 CONCLUSIONS

Our new relativistic fluid model produces interesting new results for relativistic slow-mode shocks compared to conventional relativistic MHD (Lyubarsky 2005). The downstream plasma always develops strong positive ($p_\parallel > p_\perp$) anisotropy, regardless of the isotropy of upstream plasma. Anisotropy in the relativistic system always weakens the shock (decreases the compression ratio) compared to the fully isotropic case. In some cases, the anisotropic shock is abated due to entropy considerations, while the isotropic shock remains well behaved. The strong downstream anisotropy for cases in which $\hat{\sigma} \sim 1$ leads to a firehose unstable plasma. We posit the effect of the downstream plasma being firehose unstable to be constraining the length of the reconnection current sheet, analogous to the effect of Weibel instabilities observed in PIC simulations.

REFERENCES

Asseo E., Beufils D., 1983, Ap&SS, 89, 133
Biernat H. K., Heyn M. F., Semenov V. S., 1987, J. Geophys. Res., 92, 3392
Biernat H. K., Mü hlbachler S., Semenov V. S., Erkaev N. V., Vogl D. F., Ivanova V. V., 2002, Adv. Space Res., 29, 1069
Biskamp D., 1986, Phys. Fluids, 29, 1520
Blackman E. G., Field G. B., 1994, Phys. Rev. Lett., 72, 494
Chew G. F., Goldberger M. L., Low F. E., 1956, Proc. R. Soc. Lond. A, 236, 112
Chou M., Hau L.-N., 2004, ApJ, 611, 1200
Daughton W., Karimabadi H., 2007, Phys. Plasmas, 14, 072303
Daughton W., Lapenta G., Ricci P., 2004, Phys. Rev. Lett., 93, 105004
Di Matteo T., 1998, MNRAS, 299, L15
Double G. P., Baring M. G., Jones F. C., Ellison D. C., 2004, ApJ, 600, 485
Eriksson S. et al., 2004, J. Geophys. Res., 109, A10212
Hazeltine R. D., Mahajan S. M., 2002, ApJ, 567, 1262
Hoshino M., Saito Y., Mukai T., Nishida A., Kokubun S., Yamamoto T., 1997, Adv. Space Res., 20, 973
LeFloch P. G., 1989, Shock waves for nonlinear hyperbolic systems in nonconservative form, preprint
Lyubarsky Y. E., 2005, MNRAS, 358, 113
Lyutikov M., Uzdensky D., 2003, ApJ, 589, 893
Mészáros P., 2006, Rep. Prog. Phys., 69, 2259
Petschek H. E., 1964, in Hess W. N., ed., Physics of Solar Flares, NASA Publ. No. SP-50. NASA, Washington D.C., p. 425
Shibata K., 1996, Adv. Space Res., 17, 9
Spitkovsky A., 2008, in Bassa C. G., Wang Z., Cumming A., Kaspi V. M., eds, AIP Conf. Proc. Vol. 983, 40 Years of Pulsars-Millisecond Pulsars, Magnetars, and More. Am. Inst. Phys., New York, p. 20
Swisdak M., Liu Y.-H., Drake J. F., 2008, ApJ, 680, 999
TenBarge J. M., Hazeltine R. D., Mahajan S. M., 2008, Phys. Plasmas, 15, 062112
Tolstykh Y. V., Semenov V. S., Biernat H. K., Heyn M. F., Penz T., 2007, Adv. Space Res., 40, 1538
Walthour D. W., Sonnerup B. U. Ö., Russell C. T., 1995, Adv. Space Res., 15, 501
Zel'dovich Y. B., Raizer Y. P., 2002, in Hayes W. D., Probstein R. F., eds, Physics of Shock Waves and High-Temperature Hydrodynamic Phenomena. Dover Publications, New York
Zenitani S., Hesse M., 2008, Phys. Plasmas, 15, 022101

This paper has been typeset from a TEX/LATEX file prepared by the author.